



A simplified isoprene oxidation mechanism for fast global chemistry transport modeling and emission inversion

Glenn-Michael Oomen¹, Jean-François Müller¹, Trissevgeni Stavrakou¹, Isabelle De Smedt¹, Vincent Huijnen², Flora Kluge³, Antje Inness³, and Johannes Flemming³

¹Royal Belgian Institute for Space Aeronomy (BIRA-IASB), Brussels, Belgium

²Royal Netherlands Meteorological Institute (KNMI), De Bilt, the Netherlands

³European Center for Medium-Range Weather Forecasting (ECMWF), Bonn, Germany and Reading, UK

Correspondence: Glenn-Michael Oomen (glenn-michael.oomen@aeronomie.be)

Abstract. We introduce the Simplified Isoprene Chemistry for MAGRITTE (SICMA), a compact chemical mechanism designed for computationally efficient global chemistry transport modeling and adjoint-based emission inversions. The scheme reduces the isoprene oxidation network of the MAGRITTEv1.2 model from 93 organic species and 243 reactions to four organic species and five lumped reactions. The SICMA parameters (rate coefficients and product yields) are optimized using box-model simulations across multiple NO_x regimes to reproduce cumulative formaldehyde (HCHO) production and HO_x concentrations from the full mechanism. The simplified scheme successfully captures the NO_x -dependent branching of isoprene oxidation and reproduces HCHO production and oxidant recycling with high fidelity. Implemented in the global MAGRITTE model, SICMA reproduces the monthly HCHO vertical columns from the full chemistry run within 10% over most continental regions. Larger discrepancies occur over boreal forests and remote oceans, mainly due to the simplified treatment of monoterpene oxidation and organic nitrate chemistry. Despite these simplifications, the seasonal cycle and spatial distribution of HCHO columns remain in close agreement with both the full chemistry simulation and TROPOMI observations. Inversions of isoprene emissions constrained by TROPOMI HCHO columns yield nearly identical global totals when using SICMA or the full chemistry (568.0 and 568.4 Tg yr^{-1} , respectively). SICMA therefore provides a robust and computationally efficient alternative to detailed isoprene mechanisms for large-scale modeling and emission inversion applications.

1 Introduction

Terrestrial vegetation is the largest source of volatile organic compounds (VOCs) without methane emitted into the atmosphere, with an estimated total emission source of about 1000 Tg yr^{-1} (Guenther et al., 2012). The most important biogenic VOC is isoprene (C_5H_8), which accounts for roughly half of the total biogenic VOC emissions globally, followed by monoterpenes ($\sim 15\%$), methanol ($\sim 10\%$), acetone, and other compounds. Due to their strong reactivity, biogenic VOCs play a central role in tropospheric chemistry by influencing ozone formation, hydroxyl radical (OH) recycling, and secondary organic aerosol production (Atkinson and Arey, 2003; Claeys et al., 2004). Among its oxidation products, formaldehyde (HCHO) is of particular importance, as it is a major intermediate in the oxidation of VOCs and an observable tracer for constraining isoprene emissions from space.



Table 1. Sizes of isoprene oxidation mechanisms.

Mechanism	Species	Reactions	Reference
MCM v3.3.1	602	1926	Jenkin et al. (2015)
Caltech	404	897	Wennberg et al. (2018)
RCIM	148	412	Bates and Jacob (2019)
Caltech Reduced	131	220	Wennberg et al. (2018)
MAGRITTEv1.2	93	243	Müller et al. (2019)
CRI 2.2	56	186	Jenkin et al. (2019)
IFS-COMPO	27	58	Williams et al. (2022)
AMORE-Isoprene	12	22	Wiser et al. (2023)
SICMA	4	5	this work

In the last two decades, satellite observations of HCHO have been extensively used for top-down estimates of isoprene emissions (e.g. Palmer et al., 2006; Millet et al., 2008; Stavrakou et al., 2009b, 2015; Bauwens et al., 2016; Kaiser et al., 2018; Stavrakou et al., 2018; Müller et al., 2024; Oomen et al., 2024; Li et al., 2026). Additionally, space-borne isoprene column measurements from the Cross-track Infrared Sounder (CrIS) have been used to constrain isoprene emissions (Wells et al., 2020; Li et al., 2025; Sun et al., 2025). However, the interpretation of these observations is critically dependent on the accuracy of the chemical mechanisms used to represent isoprene oxidation. Despite significant advances in laboratory and theoretical studies, the chemical complexity of isoprene oxidation remains challenging to capture in global models. Current detailed mechanisms involve hundreds of reactions and species (Jenkin et al., 2015; Wennberg et al., 2018), leading to high computational costs that restrict their use in long-term simulations, ensemble studies, and inverse modelling frameworks. As a result, most global chemistry-transport models employ reduced or lumped chemical schemes (Archibald et al., 2010). These simplified mechanisms aim to improve computational efficiency while reproducing key features of isoprene oxidation, including HCHO yields, HO_x recycling, and the sensitivity to NO_x regimes (Wennberg et al., 2018). In particular, biases in simulated HCHO columns can propagate directly into errors in inferred isoprene emissions, limiting the reliability of satellite-based constraints. Several reduced chemical schemes have been proposed in recent years, each aiming to balance chemical realism with numerical efficiency (Müller et al., 2018; Jenkin et al., 2019; Wiser et al., 2023, see Table 1).

In this work, we introduce the Simplified Isoprene Chemistry for MAGRITTE (SICMA), a compact chemical mechanism designed to efficiently represent isoprene oxidation and its impact on HCHO and oxidant budgets. SICMA is highly simplified, featuring only five lumped reactions involving four organic species with parameterized yield coefficients and reaction rates. The reaction parameters are optimized by using box-model simulations, which allows for a strong reduction of the full scheme while maintaining realistic HCHO production and HO_x recycling across different NO_x regimes.



The performance of SICMA for isoprene oxidation is evaluated using both box-model experiments and global simulations. The analysis focuses on the ability of the simplified chemistry to reproduce key chemical diagnostics, including OH, HO₂, and HCHO. The main goal of SICMA is to mimic the HCHO vertical column distribution of full chemistry simulations with the Model of Atmospheric composition at Global and Regional scales using Inversion Techniques for Trace gas Emissions (MAGRITTEv1.2, Müller et al., 2019) chemistry transport model (CTM) without the need for a large number of reactions and intermediate species, such that comparisons with space-based HCHO columns and isoprene emission inversions can be performed at lower computational cost. Furthermore, we assess the realism of simulated HCHO columns through comparison with TROPOMI HCHO satellite observations, thus providing an observational benchmark for the simplified chemistry.

We describe the TROPOMI HCHO data used for model evaluation and as constraints for VOC emission inversion in Sect. 2. Section 3 introduces the MAGRITTEv1.2 chemistry scheme used for optimizing the SICMA chemistry and the forward model and inversion setup of the CTM. Section 4 describes the SICMA scheme and the box-model experiments for parameter optimization. The SICMA chemistry skill in the MAGRITTE CTM is evaluated in Sect. 5. We summarize the implications of our findings for satellite-based constraints on isoprene emissions and future model development in the concluding section.

2 TROPOMI HCHO data

The TROPOMI HCHO product used in this study has been developed within the European Space Agency Climate Change Initiative (CCI) Precursors for Aerosols and Ozone project. Compared to the operational product, the retrieval includes several improvements in the air mass factor (AMF) calculation. In particular, a priori vertical profiles are taken from the CAMS global reanalysis (EAC4, Inness et al., 2019), ensuring temporal consistency and leading to higher HCHO columns over emission regions and lower values over background areas, thereby improving agreement with independent observations. Surface albedo is based on the high-resolution TROPOMI minimum Lambertian equivalent reflectivity climatology (Tilstra et al., 2024). The main product used here is the tropospheric HCHO column without cloud altitude correction, applying only cloud fraction filtering, as cloud corrections have limited impact on HCHO retrievals and may introduce inter-sensor inconsistencies. Updates have also been applied to the background correction and Level-2 quality assurance parameters.

The Level-3 (L3) product is provided on a $0.25^\circ \times 0.25^\circ$ grid with daily global coverage (De Smedt et al., 2025). Level-2 retrievals are filtered using the recommended quality threshold ($qa_value > 0.5$), and an additional L3 quality flag is used to exclude grid cells with insufficient valid observations. For each grid cell, the dataset provides the tropospheric HCHO column (`tropospheric_HCHO_column_number_density_clear`) together with intermediate quantities, including slant columns, background-corrected slant columns, AMFs (with and without cloud correction), averaging kernels, and auxiliary parameters such as a priori vertical profiles, surface albedo and cloud properties. Mean random and systematic uncertainties are reported, along with statistical indicators such as intra-cell standard deviations. Averaging kernels are used in this work to apply vertical smoothing when comparing model simulations with satellite observations.

The dataset has been evaluated against ground-based Fourier Transform Infrared (FTIR) measurements, leading to a global-scale bias correction based on the regression relationship ($y = 1.315x - 0.934$). In addition to the quality flag applied to

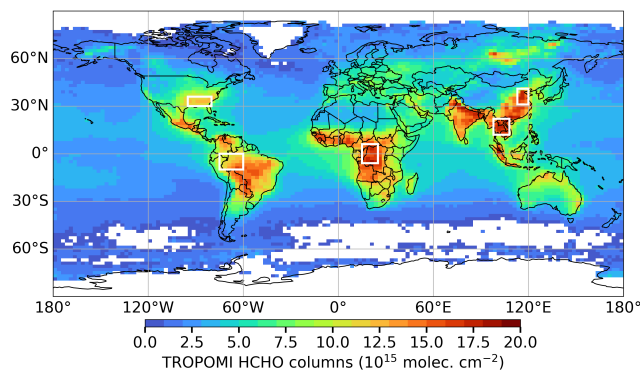


Figure 1. Average TROPOMI HCHO columns for the year 2019 from the ESA CCI HCHO product. White rectangles denote regions that will be used for model comparisons in Sect. 5.

the L3 data, we require a minimum of 4 days with valid data per grid cell per month, and we filter low HCHO columns $< 0.65 \times 10^{15}$ molec. cm^{-2} . The resulting ground-based bias-corrected HCHO columns, depicted in Fig. 1, are used both for model evaluation and as observational constraints in the inversion system. Further details on the product and its validation are provided in the CCI Algorithm Theoretical Basis Document (Van Roozendael et al., 2026) and the Product Validation and Intercomparison Report (Compernelle et al., 2025).

3 MAGRITTEv1.2 chemistry transport model

3.1 Chemical reaction network

The simplified chemistry scheme with parametrized reaction rates and coefficients is based on the chemical reaction mechanism of the MAGRITTEv1.2 CTM (see Müller et al., 2019, for an in-depth description), which has an extensive, up-to-date isoprene oxidation chemistry primarily based on the Leuven Isoprene Model (LIM, Peeters et al., 2009, 2014) and the Caltech oxidation mechanism (Wennberg et al., 2018). As in Oomen et al. (2024), the isomerization rates of the δ -hydroxyperoxy radicals from isoprene oxidation by OH are enhanced, relative to the MAGRITTEv1.1 mechanism, in order to provide a better match with chamber data (Novelli et al., 2020). The reaction network comprising the oxidation of isoprene and its intermediate products contains 243 reactions and uses 93 different compounds (Table 1). The oxidation reactions of monoterpenes (i.e. α -pinene) adds another 14 reactions to this number.

3.2 Forward simulation setup

The MAGRITTE CTM calculates the chemical interactions and transport of chemical compounds in the atmosphere based on a priori emission information. The model can be run in global ($2 \times 2.5^\circ$) or regional configuration ($0.5 \times 0.5^\circ$) using lateral



95 boundary conditions from the global model run. The vertical resolution of the model consists of 40 levels from the surface up to the lower stratosphere at 44 hPa following a σ -level coordinate system.

Meteorological fields used in the model are taken from ERA5 reanalysis data (Hersbach et al., 2020). The aerosol optical depth data is obtained from the CAMS global reanalysis (Inness et al., 2019). The model uses gridded emission data from bottom-up inventories: MEGAN-MOHYCAN for biogenic emissions (Stavrakou et al., 2018), CAMS-GLOB-ANTv5.3 for anthropogenic emissions (Soulie et al., 2024), and QFEDv2.4 for biomass burning emissions (Darmenov and da Silva, 2015), with emission factors from Andreae (2019). The annual global NMVOC emission estimates for 2019 amount to 439 Tg for isoprene, 108 Tg for monoterpenes, 112 Tg for biogenic methanol, 193 Tg for anthropogenic VOCs, and 93 Tg for biomass burning VOCs. The model also includes oceanic emissions of methanol, acetone and acetaldehyde (Müller et al., 2019), and accounts for both wet scavenging by cloud and rain droplets (Stavrakou et al., 2009a) and dry deposition (Müller et al., 2018).

105 The MAGRITTE model is run for the year 2019 with a 6-month spin-up time. It accounts for diel variations in chemical compounds through correction factors on the chemical reaction rates, photolysis rates, convective fluxes, and boundary layer diffusion coefficients computed by a simulation using a time step of 20 min (Stavrakou et al., 2009b). The model is run with a time step of 24 h using daily averaged chemical and dynamical parameters adjusted for the diurnal cycle using the pre-calculated correction factors.

110 3.3 Inversion setup

The inversion system of MAGRITTE relies on the adjoint-based approach to optimize the gridded emissions of biogenic, anthropogenic, and pyrogenic sources, constrained by TROPOMI HCHO data over land. The setup has been described in detail in previous publications (e.g. Oomen et al., 2024; Müller et al., 2024; Opacka et al., 2025; Sfindla et al., 2026). Here we perform a global emission inversion, in which continental emissions are optimized per emission category (biogenic, anthropogenic, pyrogenic), per grid cell, per month, for a total of $3 \times 90 \times 144 \times 12 \times 0.3 = 139950$ emission parameters. Grid cells with NMVOC emissions below 10^{10} molec. cm⁻² s⁻¹ throughout the year are not optimized. Additionally, we require at least 10 valid satellite observations per $2 \times 2.5^\circ$ grid cell per month. Consequently, the total number of optimized emission parameters is reduced to approximately 76 000.

120 Model columns are computed by running MAGRITTE in forward mode for a given set of emission parameters \mathbf{f} . The cost function J is calculated as

$$J(\mathbf{f}) = \frac{1}{2} \left[(\mathbf{H}(\mathbf{f}) - \mathbf{y})^T \mathbf{E}^{-1} (\mathbf{H}(\mathbf{f}) - \mathbf{y}) + \mathbf{f}^T \mathbf{B}^{-1} \mathbf{f} \right], \quad (1)$$

where $\mathbf{H}(\mathbf{f})$ are the model columns, \mathbf{y} are the observed TROPOMI HCHO columns, and \mathbf{E} and \mathbf{B} are the error covariance matrices of the emissions and observations, respectively. In the comparison of model columns to observations, the vertical sensitivity of the satellite is taken into account by applying averaging kernels to the model profiles. Additionally, the modeled monthly columns are based on daily values at the satellite overpass time ($\sim 13:30$ local time), while accounting for the number of observations for each day.



Table 2. Simplified reaction scheme for the chemical oxidation of isoprene. It involves eleven parameters (α to ζ , k_1 to k_5). The blue font denotes parameters that are optimized using box-model simulations. The production of HO_x radicals from these reactions is optimized simultaneously in R2, R3, and R5 (cf. Sect. 4.2). Details about the reaction rates are given in this section and in Table 3.

#	Reactions	Rates
R1	$\text{ISOP} + \text{OH} \rightarrow \text{ISOPO}_2$	k_1
R2	$\text{ISOPO}_2 + \text{HO}_2 \rightarrow \alpha \text{ IOX} + \beta \text{ HCHO} (+ \text{inorg.})$	k_2
R3	$\text{ISOPO}_2 + \text{NO} \rightarrow \gamma \text{ IOX} + \delta \text{ HCHO} (+ \text{inorg.})$	k_3
R4	$\text{ISOPO}_2 \rightarrow \epsilon \text{ IOX} + \text{inorg.}$	k_4
R5	$\text{IOX} + \text{OH} \rightarrow \zeta \text{ HCHO} (+ \text{inorg.})$	k_5

The cost function in Eq. 1 is minimized using a quasi-Newtonian algorithm, in which its gradient with respect to the emission parameters is calculated using the adjoint of the MAGRITTE model (Müller and Stavrou, 2005). The convergence criterion is reached when the norm of the gradient of the cost function is reduced by a factor of 100 with respect to its initial value. This typically occurs after around 30 iterations.

4 Simplified chemistry model: SICMA

4.1 Isoprene oxidation scheme

One of the limitations of adjoint-based inversions of isoprene emissions is the complex chemistry involved and its associated high computational cost. Here we simplify the chemical degradation of isoprene from 93 species and 243 reactions in the MAGRITTEv1.2 mechanism to a strongly reduced network. The structure we propose is shown in Table 2 and consists of five reactions. The first reaction, i.e. the oxidation of isoprene by OH (R1), produces a short-lived peroxy radical, ISOPO_2 , and its reaction rate (k_1) is well constrained from experimental data (Burkholder et al., 2015). Next, we include three reactions that represent the three main channels through which the peroxy radical can react: $\text{ISOPO}_2 + \text{HO}_2$ (R2), $\text{ISOPO}_2 + \text{NO}$ (R3), and an isomerization reaction (R4). The HO_2 -pathway and isomerization are important in low- NO_x environments, whereas the NO -pathway prevails in high- NO_x conditions.

In the full MAGRITTE mechanism, the reaction channels highlighted above produce a variety of intermediate oxidation products. Here, we lump all intermediate oxidation products (besides HCHO) into a unique intermediate oxidation compound (IOX). The yields of HCHO and IOX from the reactions of ISOPO_2 are parameterized using the adjustable parameters α , β , γ , δ , and ϵ . Among these parameters, β and δ account for primary HCHO production, whereas the other parameters quantify the delayed HCHO production via IOX. The reaction rates k_2 and k_3 are taken from the recommendations of Wennberg et al. (2018). The rate of the isomerization (k_4) is derived from the bulk 1,6 H-shift rates of the pool of isoprene peroxy radicals adopted in the MAGRITTEv1.2 mechanism (Müller et al., 2019). The weighted average at 298 K and typical conditions for the Amazon (30 ppt NO and 20 ppt HO_2) is 0.0089 s^{-1} . The last reaction is the oxidation of IOX by OH, to form HCHO, repre-



150 sending the secondary, delayed HCHO production from isoprene. The reaction rate k_5 will be optimized based on comparisons with the full MAGRITTEv1.2 chemistry model.

An important aspect in isoprene oxidation chemistry is its feedback on the oxidizing capacity of the atmosphere. Isoprene emissions have a strong impact on OH and HO₂ concentrations. However, the reactions of OH and HO₂ with the organic peroxy radicals generated in the mechanism are numerous, and also a significant amount of recycling takes place. In order to tackle this problem, we include a production of OH and HO₂ in the reactions ISOPO₂ + HO₂, ISOPO₂ + NO, and IOX + OH, with adjustable coefficients (R2, R3, and R5, see Table 2). For the isomerization reaction, the yields of OH and HO₂ are derived from the corresponding 1,6 H-shift reactions of the MAGRITTE model.

4.2 Parameter optimization

160 In order to optimize the parameters of the chemistry network shown in Table 2, we use box model simulations with the kinetic pre-processor (KPP) package (version 3.0.2, Sandu et al., 2023). The list of reactions of MAGRITTEv1.2 chemistry is loaded into the KPP system, which runs the chemical evolution over time.

In the simulations, we adopt Master Chemical Mechanism (MCM) photolysis rates based on solar zenith angles in typical Amazonian conditions (i.e., 10° S, on the 15th of July), and the temperature is fixed to 298 K. The initial volume mixing ratios for H₂O, CO, and ozone are set to 1%, 150 ppb, and 15 ppb, respectively. To avoid HCHO production from methane, its concentration is set to zero. Since isoprene oxidation pathways are NO_x-dependent, we perform box model simulations at three different initial NO_x concentrations: 0.03 ppb, 0.3 ppb, and 3 ppb. At every 6-min time step, we require the total NO_x (= NO + NO₂) to remain constant. Finally, we force the concentration of isoprene to a diurnal profile with a maximum of 1 ppb at noon. This approximates a continuous emission of isoprene throughout the day, peaking at noon, and no emissions at night. In box model simulations of the MAGRITTEv1.2 full chemistry, a diurnal concentration profile of monoterpenes is included, similar to that of isoprene but with 10-times lower values, corresponding to the monoterpene-to-isoprene molar emission ratio for Amazonia (Sindelarova et al., 2022). Given the similarly short atmospheric lifetimes of isoprene and monoterpenes, the simplified chemistry scheme will therefore represent the total yield of HCHO from combined isoprene and monoterpene emissions, for the case of 10% monoterpene-to-isoprene molar emission ratio. This representation is necessarily simplified and does not explicitly account for differences in emission patterns or chemical degradation pathways between isoprene and individual monoterpene species.

175 We first perform box model calculations with the MAGRITTEv1.2 chemistry. The simulation starts at 9 am local time and runs for 84 hours with a time step of 6 minutes. We track the total HCHO production from both isoprene and monoterpenes, illustrated in Fig. 2, for different NO_x concentrations. Since the isoprene and monoterpene concentrations are fixed in the box model, the cumulative HCHO production (Fig. 2a) strongly increases with increasing NO_x, mainly due to the higher concentration of OH (Fig. 2c).

180 The optimization of the parameters of Table 2 is constrained by the MAGRITTEv1.2 chemistry run based on the HCHO production (Fig. 2a) and the concentrations of OH and HO₂ (Fig. 2d,e). These parameters account for the chemical feedbacks between the organic and inorganic chemistry. Indeed, the OH concentration has a strong impact on the rates of reactions R1

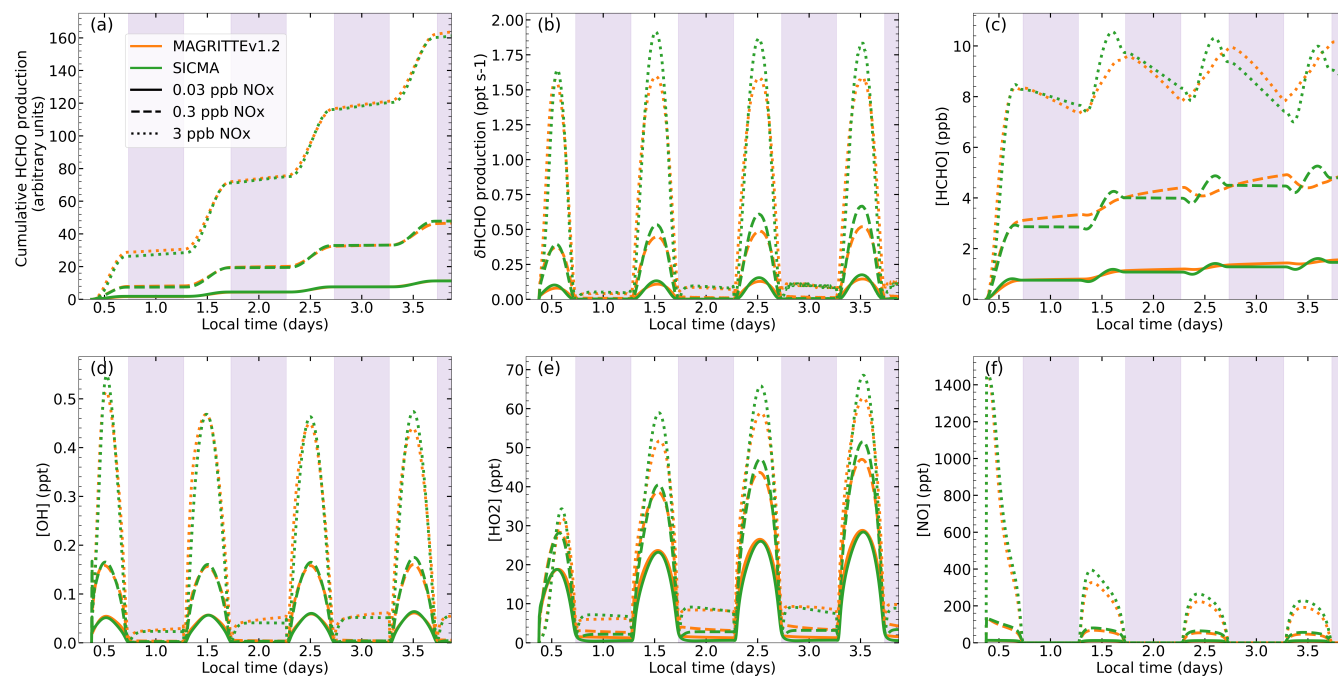


Figure 2. Comparison of box model simulations of MAGRITTEv1.2 (orange) and SICMA (green) chemistry for cumulative HCHO production (a), instantaneous HCHO production (b), concentration of HCHO (c), OH (d), HO₂ (e), and NO (f). Each panel shows runs with 0.03 ppb (solid line), 0.3 ppb (dashed line), and 3 ppb (dotted line) total NO_x concentrations. Nighttime is defined as 17.30–6.30 local time and is denoted by the shaded area. Panels a, d, and e are used for optimizing the parameters as described in Sect. 4.2.

and R5, whereas the HO₂ and NO concentrations determine the dominant reaction pathway of ISOP₂ in R2 and R3. The NO₂ yield from the reaction of ISOP₂ with NO (R3) is set to 0.87, in order to account for organic nitrate formation (Müller et al., 2019). The precise value of this yield is unimportant in the box model runs with fixed NO_x levels, but it will play an important role in the chemistry-transport model simulations. For OH and HO₂, regeneration occurs in each reaction, hence this needs to be accounted for in R2–R5. These yields are constrained in the optimization by the OH and HO₂ concentrations of the full MAGRITTEv1.2 chemistry box-model simulations, and through their feedback on the HCHO chemistry (Fig. 2). Likewise, the IOX production impacts the OH budget.

We used a Nelder-Mead simplex optimization method (Gao and Han, 2012) from the SciPy library to determine the minimum of the total normalized least squares difference in the cumulative HCHO distributions, OH concentrations, and HO₂ concentrations from the MAGRITTEv1.2 and SICMA chemistry runs (Figs. 2a,d,e). The initial guess of each of the coefficients of the organic parameters (α to ζ) is set to 1.0, and the initial guess of the IOX oxidation reaction (k_5) to 10^{-11} s⁻¹. For the stoichiometric coefficients of OH and HO₂, the initial guess is set to 0.5. The convergence tolerances in the minimization algorithm are set to 0.01 in absolute values for the parameters. Convergence in parameter estimation is reached after roughly 200 simplex iterations. The optimized isoprene reactions of the SICMA chemistry are presented in Table 3.



Table 3. Same as Table 2, but with the optimized parameter values, including the HO_x production stoichiometric coefficients. *T* in the rate expressions denotes the temperature in Kelvin.

#	Reactions	Rates (in s ⁻¹)
R1	ISOP + OH → ISOPO2	$3.0 \times 10^{-11} \exp(360/T)$
R2	ISOPO2 + HO ₂ → 1.85 HCHO + 1.05 OH + 0.43 HO ₂	$2.1 \times 10^{-13} \exp(1300/T)$
R3	ISOPO2 + NO → 3.72 IOX + 0.61 HCHO + 0.87 NO ₂ + 1.01 HO ₂	$2.7 \times 10^{-12} \exp(350/T)$
R4	ISOPO2 → 0.61 IOX + 0.2 OH + 0.75 HO ₂	$1.16 \times 10^{11} \exp(-9000/T)$
R5	IOX + OH → 0.56 HCHO + 0.99 HO ₂	5.60×10^{-12}

Figure 2 shows the comparison of key compounds in the box model simulations. The cumulative HCHO productions of the two chemistry schemes are in excellent agreement, considering the low complexity of the SICMA scheme. The instantaneous HCHO production in Fig. 2b shows slight differences, with a higher HCHO production in SICMA around noontime and lower production during mornings and evenings. These differences in HCHO production, along with differences in OH concentration (during the night), result in HCHO diurnal profile differences, as shown in Fig. 2c. However, the magnitude of HCHO concentrations is well reproduced.

The parameter optimization is also constrained by OH and HO₂ concentrations. The simplified chemistry scheme performs well in reproducing the OH and HO₂ concentrations, although the nighttime concentrations in the SICMA runs are slightly lower at low NO_x due to the lack of OH and HO₂ recycling compared to the more complex MAGRITTE mechanism. In the low-NO_x regime, OH is recycled through the ISOPO2 + HO₂ reaction. At high NO_x, however, very little OH recycling takes place (besides HO₂ + NO) in the full MAGRITTEv1.2 chemistry, hence no OH recycling is needed from reaction R3 (Table 3). Instead, the high IOX yield (3.72) in the reaction with NO (R3) leads to more OH titration, which depletes OH and forms HCHO and HO₂ via reaction R5. As a result, the simplified chemistry scheme succeeds well in reproducing the evolution of key species of isoprene oxidation like HCHO, OH, and HO₂. The NO concentration is also well reproduced, except for a small overestimation due to the lower number of organic peroxy radicals considered in SICMA, compared to the full chemistry.

5 Evaluation of SICMA in the MAGRITTE CTM

The goal of the simplified chemistry is to reproduce HCHO columns generated using a comprehensive isoprene emission chemistry, in order to improve computational performance of chemistry transport modelling and data assimilation approaches. Here, we explore the use of SICMA (Table 3) within the chemistry transport model MAGRITTE. We replace the suite of reactions related to the oxidation of isoprene and monoterpenes by the five parameterized reactions, and evaluate its performance against full chemistry simulations for 2019. Reactions related to other VOCs are identical in the two simulations. Similarly, the inorganic chemistry and photolysis rates are taken from the full chemistry.

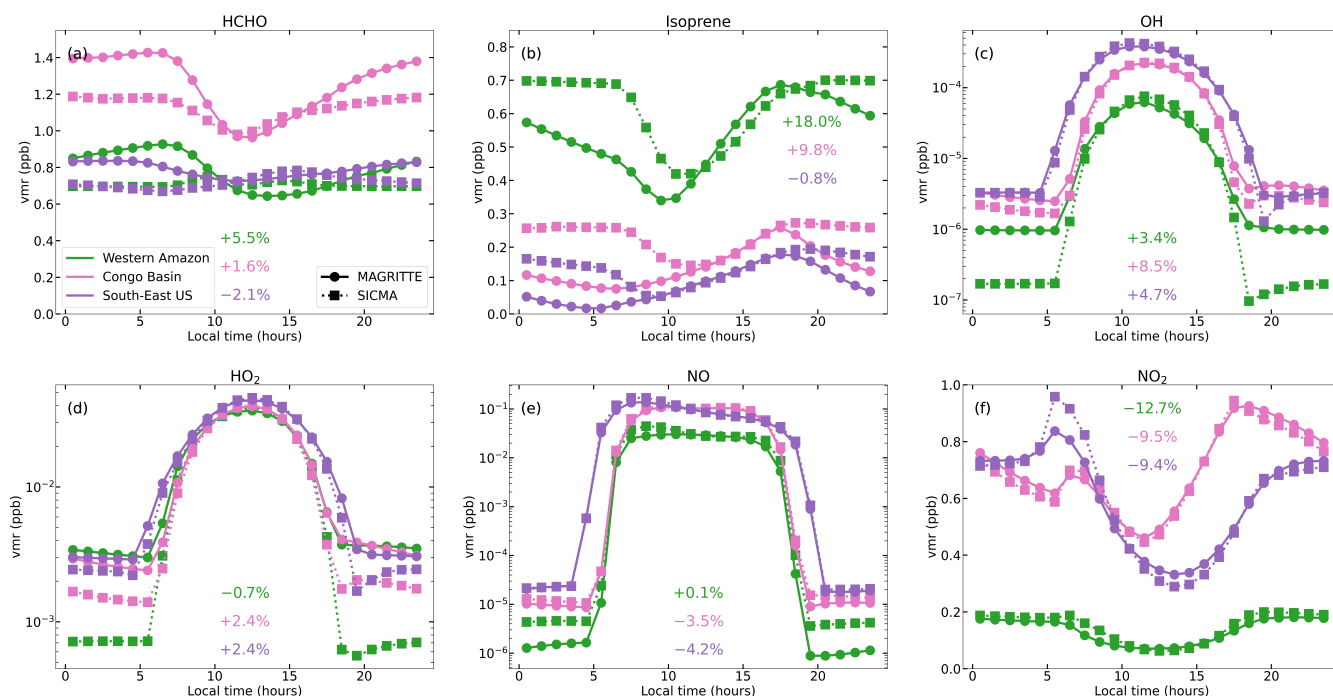


Figure 3. Monthly-averaged diurnal cycles of HCHO (a), isoprene (b), OH (c), HO₂ (d), NO (e), and NO₂ (f) mixing ratios. Each panel depicts hourly concentrations vertically-averaged from the surface up to 1 km altitude, for July 2019. Three regions are considered (see Fig. 1): Western Amazon (0 – 10° S, 60 – 75° W) in green, the Congo Basin (6° S–6° N, 15 – 25° E) in pink, and South-East US (30 – 36° N, 80 – 95° W) in purple. Solid and dotted lines denote results obtained using respectively the full MAGRITTE chemistry and the SICMA scheme. Values shown inset each panel correspond to the monthly-averaged relative difference of the daytime (9–15 h local time) concentrations for the three regions, calculated as (SICMA – MAGRITTE)/MAGRITTE (in %).

5.1 Diurnal cycles

220 We evaluate the diurnal cycles for HCHO, isoprene, OH, HO₂, NO, and NO₂ in Fig. 3. We have selected three prominent
 isoprene emitting regions depicted in Fig. 1: the Western Amazon rain forest, the Congo Basin, and South-East US. Western
 Amazonia is characterized by high isoprene emissions and columns paired with generally low NO_x concentrations. The Congo
 Basin presents a similar environment (evergreen broadleaf rain forest) but with generally higher NO_x levels and therefore
 higher OH and lower isoprene columns. Finally, the South-East US is characterized by a strong seasonality and by the presence
 225 of anthropogenic emissions leading to high NO_x and OH concentrations.

For HCHO, there is good agreement in the magnitude of the concentration in the planetary boundary layer for the different
 regions, especially around noon time. Similar to the box model simulations, there is a discrepancy in the shape of the diurnal
 profile, which is partly due to the difference in nighttime OH (Fig. 2c). The SICMA mechanism leads to lower nighttime OH
 and HO₂, likely due to the absence of ozonolysis reaction of isoprene and monoterpenes (Paulson and Orlando, 1996). Lower



230 OH concentrations, in combination with the absence of the ISOP + O₃ reaction, results in higher isoprene and lower HCHO concentrations during the night in the SICMA results.

During the day, the two mechanisms produce similar results for all compounds. For NO₂, the SICMA chemistry leads to lower concentrations by about 10% between 9 and 15 h local time, whereas the NO levels from MAGRITTE and SICMA are more similar. This difference is caused by the larger number of organic peroxy radicals in the full mechanism, leading to a stronger conversion of NO to NO₂. The OH concentrations, on the other hand, are slightly too high during the day (~5%). This, in combination with increased isoprene concentrations during the night, is responsible for the decline of the morning isoprene concentrations in SICMA. Nevertheless, the overall performance of the SICMA chemistry is adequate to replicate the full MAGRITTE results, especially during the day, despite its simplicity.

5.2 Evaluation of the global model

240 Figure 4 shows a comparison of annually-averaged HCHO column distributions from global model simulations using either the full or simplified chemistry. The distributions agree very well in biogenic source regions, where the isoprene chemistry matters most, as well as in anthropogenically dominated and remote regions, where isoprene plays a negligible role. The magnitude of HCHO columns are in good agreement, within 10%, over continents. Over oceans, the HCHO columns of the simplified chemistry are up to 15% too low due to the neglect of organic nitrate and peroxyxynitrate formation in the SICMA mechanism. In particular, peroxyacetyl nitrate (PAN) is formed from the oxidation of many hydrocarbons including isoprene. PAN and other organic NO_x reservoirs act as carriers of NO_x away from the emission sources. The average westward outflow from trade winds leads to higher NO_x levels over the ocean in the full chemistry run (see Fig. 5e,f). This in turn leads to higher OH concentrations over remote regions, and hence to larger background HCHO production from methane oxidation, though the difference in absolute HCHO columns between the two models is small ($< 5 \times 10^{14}$ molec. cm⁻²).

250 To evaluate the differences between the two chemical schemes in the CTM, we show difference maps for key compounds in Fig. 5. Over continents, the differences in OH concentrations are relatively small, generally of the order of 10% or less. The OH concentrations of the simplified chemistry are slightly higher than those of the full chemistry, the exception being the remote desert areas where the long-range transport of NO_x reservoirs leads to higher NO_x levels in the MAGRITTE simulation. However, an important difference arises in boreal forests, where the SICMA OH overestimation ranges between 10 to 20%. This difference can be explained by the fact that monoterpene chemistry is omitted in the SICMA mechanism. Over needleleaf boreal forests, characterized by high monoterpene emissions, the isoprene-to-monoterpene emission ratio is a factor of 3 to 10 lower than assumed in SICMA. The oxidation of monoterpenes represents a significant NO_x sink due to organic nitrate formation (Müller et al., 2019), estimated at about 1.5 Tg(N) yr⁻¹ globally in the MAGRITTE model run. A large fraction of the formed organic nitrate is lost through aerosol uptake or deposition, or transported away from source regions, resulting in reduced NO_x and OH levels, in particular over eastern Siberia and boreal America. The general impact of using the SICMA mechanism in HCHO columns in the region is limited (Fig. 5a) due to competition between the lower formation of HCHO through monoterpene oxidation and the increased background source from methane due to higher concentrations of

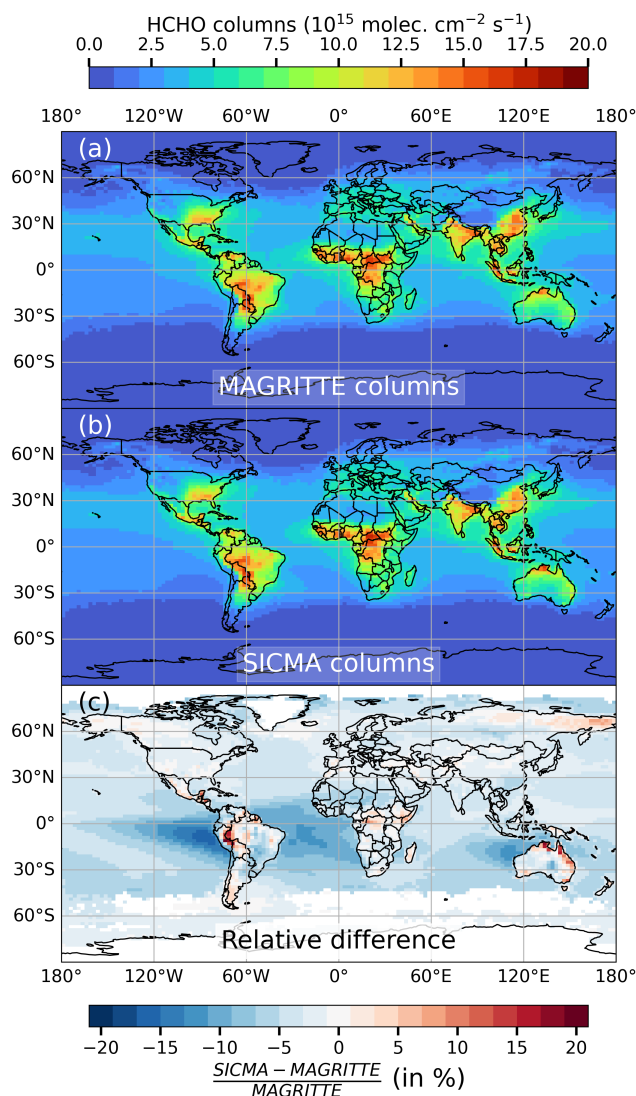


Figure 4. Simulated HCHO columns of forward MAGRITTE CTM runs using either the full MAGRITTEv1.2 isoprene chemistry (a) or the simplified SICMA scheme (b). The HCHO columns have been collocated with TROPOMI HCHO observations and averaging kernels have been accounted for in the comparisons between the model and the observations of Fig. 1. Panel c shows the relative difference between the top panels, in %.

OH. However, the higher OH concentrations also reduce the lifetime of isoprene, leading to lower isoprene columns using the SICMA chemistry in the boreal forests.

265 The ratio of isoprene-to-monoterpene also plays an important role in tropical regions, which are the main source of biogenic volatile organic compounds worldwide. A clear spatial correlation is found between the emission ratio of the MEGAN-

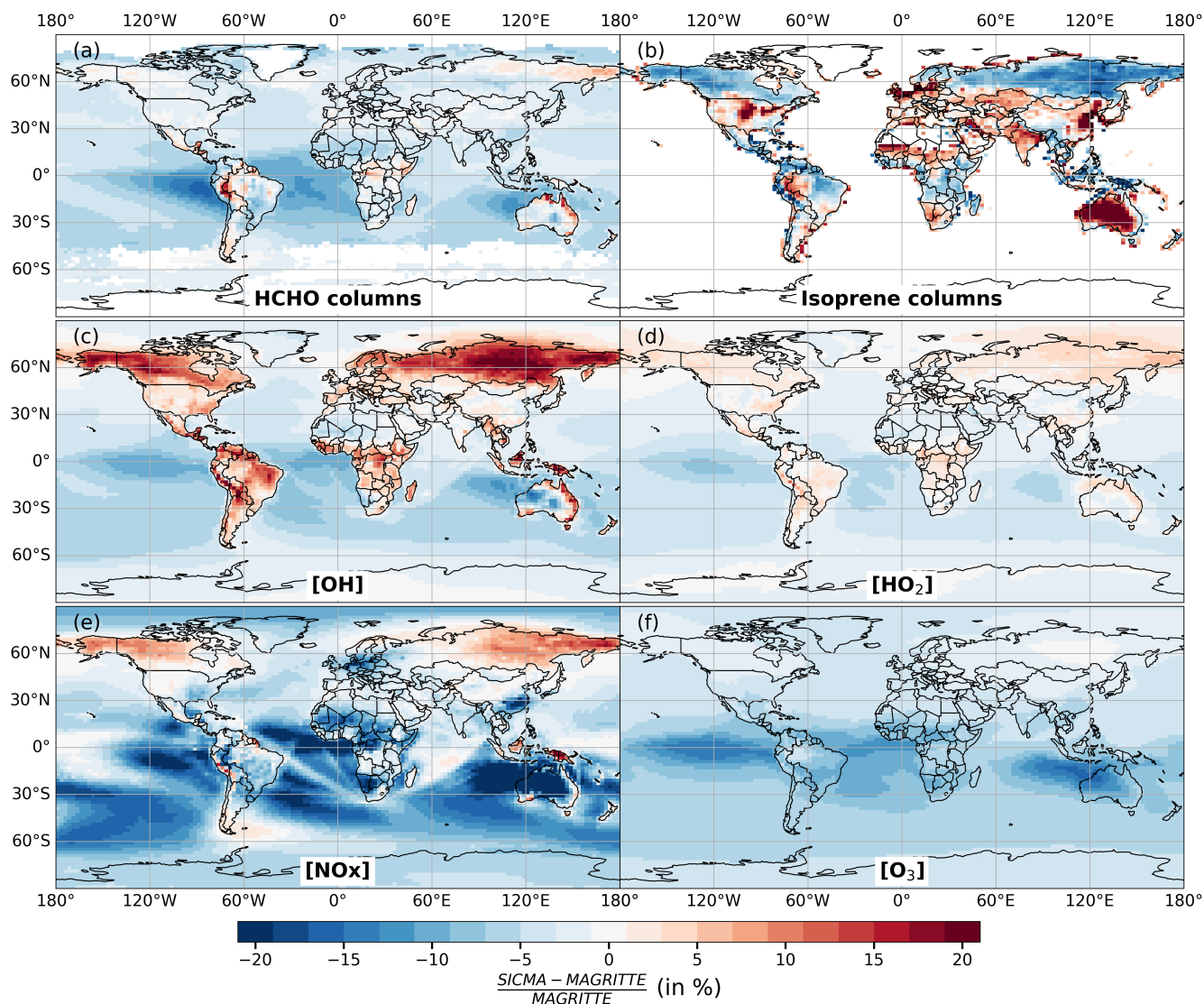


Figure 5. Differences (in %) between MAGRITTE and SICMA chemistry runs for HCHO (a), isoprene (b), OH (c), HO₂ (d), NO (e), and NO₂ (f). For HCHO and isoprene, the differences are shown for the total vertical column, at 13:30 local time, and TROPOMI averaging kernels have been applied for HCHO. For isoprene, pixels with columns below 3×10^{12} molec. cm⁻² have been omitted for clarity. The other panels show differences for the averaged daytime (9–17 local time) concentrations below 1 km altitude.

MOHYCAN inventory (Fig. S1), which is used as input for forward simulations, and the HCHO column discrepancy between MAGRITTE and SICMA displayed on Fig. 5a. In areas with high monoterpene emissions, the SICMA HCHO columns are generally underestimated, and vice versa. However, the differences are generally much lower than 10% locally.



270 The differences in isoprene columns, illustrated in Fig. 5b, are mainly driven by differences in OH concentration, since
reaction with OH is by far the main sink of isoprene (Wennberg et al., 2018). Increases in OH concentration therefore increase
the reactivity of isoprene and lower the isoprene columns. The changes in isoprene columns and in OH concentrations (averaged
below 1 km) are generally of opposite sign and display the same patterns, especially in high-emission areas (Fig. 5b-c). The
correspondence is not perfect, because the isoprene column is mostly sensitive to OH levels close to the surface, such that the
275 1 km average might not always reflect the isoprene reactivity. In areas with low isoprene columns, like central US and the
North China Plain, the impact of the SICMA mechanism is almost negligible on the 1 km OH average but might be significant
near the surface, leading to large relative differences in the isoprene columns. However, the absolute difference between the
two chemical schemes in these areas is small ($< 2 \times 10^{13}$ molec. cm^{-2}).

The modeled HCHO columns using the two mechanisms exhibit very similar seasonality, as shown in Fig. 6. The monthly
280 variability is mainly driven by the emissions and meteorology, which are identical for both simulations. The impact of isoprene
chemistry on the temporal evolution is small. Over Amazonia (Fig. 6a), the HCHO columns from SICMA are overall higher
by about 7%, due to the higher isoprene-to-monoterpene ratio in this region, leading to a slight overestimation of the HCHO
yield from the simplified chemistry.

Both model results show also a good agreement in temporal variation with TROPOMI HCHO observations, consistent
285 with previous comparisons of MAGRITTE columns with TROPOMI data (Sfendla et al., 2026). In the Congo basin, both
models consistently underestimate the HCHO columns by about 20%. In Amazonia, the magnitude of the columns is very well
reproduced, except for a $\sim 10\%$ underestimation during the dry season in August and September. In South-East US, we observe
a clear separation of summer and winter seasons, with an amplitude of about factor of five. In North China Plain and South-East
Asia, the observed HCHO columns are higher during summer/dry season conditions compared to the model. Although this is
290 arguably caused by uncertainties in the bias correction applied to the satellite HCHO product (Sect. 2), the high summertime
HCHO columns are corroborated by ground-based validation campaigns, such as FTIR (Vigouroux et al., 2020), MAX-DOAS
(De Smedt et al., 2021), and Pandora stations. During winter/wet season, the bias between model and satellite observations is
much smaller.

5.3 Evaluation of the emission inversion

295 In this section, we show the results of emission inversions constrained by TROPOMI data (Fig. 1) using either the full
MAGRITTEv1.2 chemistry or the simplified isoprene oxidation chemistry described in Table 3 in the MAGRITTE model.
In the majority of source regions, the a priori model columns are on average lower than the observed TROPOMI HCHO
columns shown in Fig. 6. Both inversions consistently suggest an increase of the a priori MEGAN-MOHYCAN isoprene emis-
sions from 439 Tg to 568 Tg on global scale (Fig. 7 and Table 4), whereas Fig. 8 shows the relative difference in top-down
300 emissions between the inversion using the MAGRITTEv1.2 and SICMA isoprene chemistry. The overall difference is small,
although locally both over- and underestimations of isoprene emissions are found, reaching up to 20%.

The relative difference of the top-down isoprene emissions (Fig. 8) is similar but of opposite sign to the relative differ-
ence in the HCHO column simulated using bottom-up isoprene emissions (Fig. 5a). In regions where the SICMA chemistry

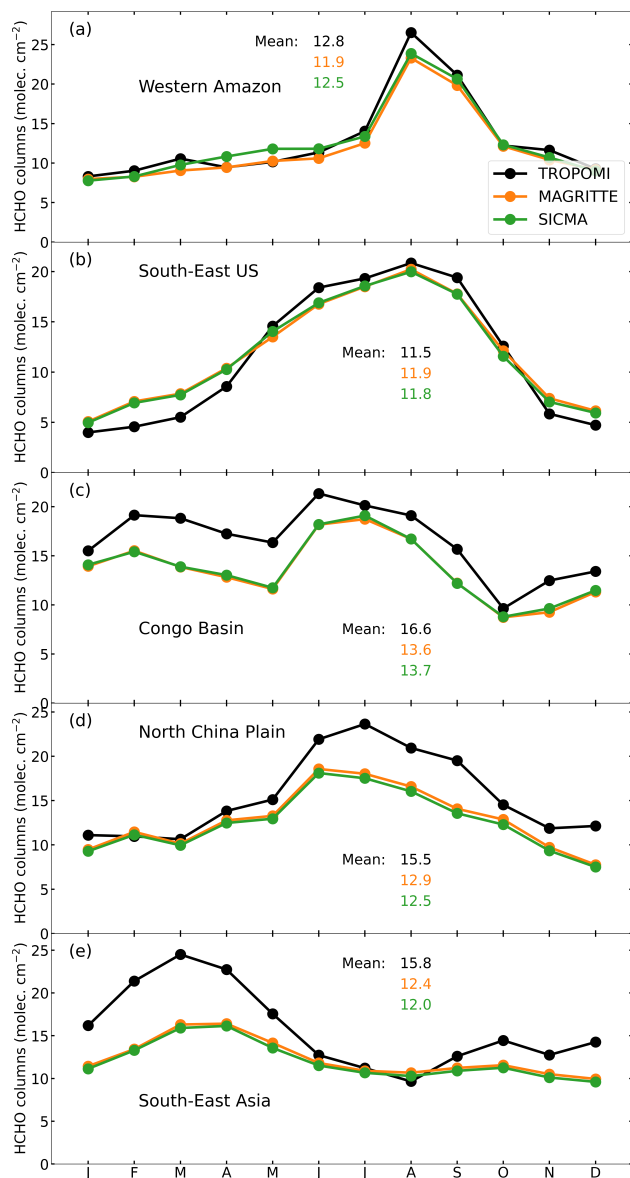


Figure 6. Monthly time series of HCHO columns for Western Amazon, South-East US, Congo Basin, North China Plain, and South-East Asia (from top to bottom) in the year 2019. The large regions are defined in Fig. 1. The lines correspond to TROPOMI HCHO columns (black), full chemistry HCHO model columns (orange), and simplified chemistry model HCHO columns (green).

produces lower HCHO columns, the isoprene emission change is stronger after inversion, and vice versa, compared to the
 305 MAGRITTEv1.2 chemistry. This can also be seen in the isoprene emission time series over selected regions shown in Fig. 9. In
 regions with higher modeled HCHO columns using SICMA chemistry (e.g., Western Amazonia), the top-down isoprene emis-
 sions are slightly lower (by 10%). In South-East US, a priori HCHO columns during summer (May to September) are lower

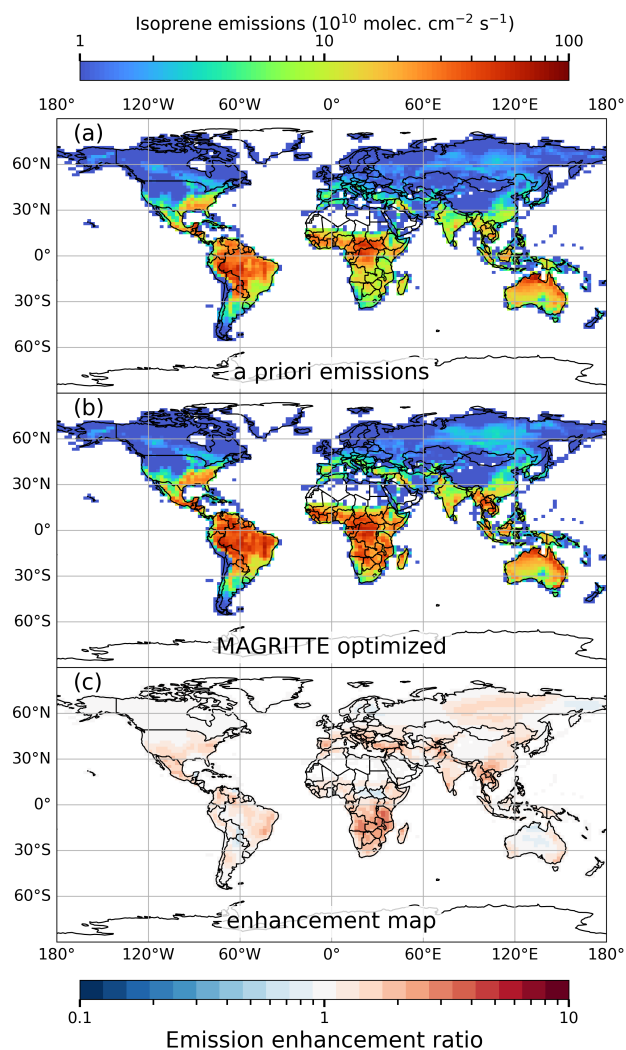


Figure 7. Isoprene emissions from the MEGAN-MOHYCAN biogenic emission inventory (a), and derived from an emission inversion using the MAGRITTEv1.2 chemistry (b), averaged for the year 2019. Panel c shows the emission enhancement map, calculated as the ratio of panel (b) over panel (a).

than TROPOMI HCHO, which leads to an overall increase in isoprene emissions, and an excellent agreement between the results of the simplified and the full chemistry. In the Congo basin the emissions inferred from both inversions agree very well (Fig. 9c) across the seasons, and are enhanced compared to the a priori estimates. Similar conclusions are drawn for the North China Plain, a region dominated by anthropogenic VOC emissions (Fig. 6d). For South-East Asia, the high TROPOMI HCHO columns observed during the dry season (March to May, Fig. 6e) drive the strong increases of top-down isoprene emissions, which are a factor of two higher than the a priori. Biomass burning VOC emissions are also increased in this area (Fig. S2).

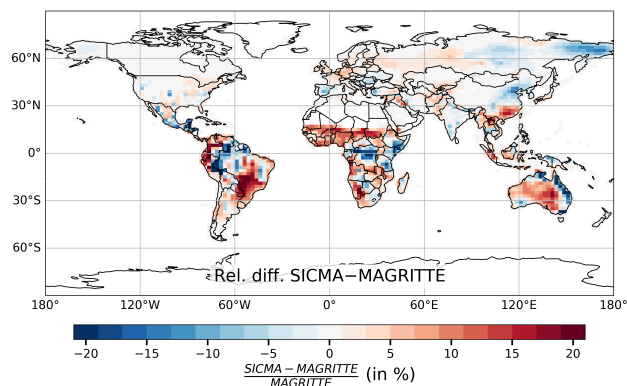


Figure 8. Relative difference in isoprene emissions after emission inversion using MAGRITTEv1.2 and SICMA chemistry in the MAGRITTE CTM.

Overall, for all selected regions, the inferred isoprene emissions from the inversion using SICMA or the MAGRITTEv1.2
315 chemistry show a very close agreement, both in terms of magnitude and seasonal variability.

Globally, the inversion leads to a large biogenic emission enhancement of almost 30% for both inversions (Table 4). In
spite of the small differences between the predictions of the two model simulations (Fig. 4) for HCHO and isoprene columns,
the difference in top-down isoprene totals is negligible. There is also good agreement with respect to biomass burning VOC
emissions, both regionally and globally. The anthropogenic VOC emissions inferred from the SICMA inversions are 8% higher
320 compared to the full chemistry results (Table 4). This can be attributed to the moderately lower a priori HCHO columns of the
SICMA simulation in northern mid-latitudes, and in particular over Europe and eastern China (Fig. 4), where anthropogenic
VOCs are an important HCHO source. Consequently, the derived anthropogenic VOCs in SICMA are higher to compensate
for the lower biogenic contribution.

6 Conclusions

325 We developed SICMA, a highly reduced representation of isoprene oxidation for the MAGRITTE chemistry-transport model.
The impact of monoterpenes is also crudely accounted for in the parameterization, by assuming a 10% molar ratio relative to
isoprene abundance. The mechanism condenses 93 organic species and 243 reactions into four organic species and five lumped
reactions in which HCHO production and HO_x recycling is parameterized. Box-model optimization across low-, intermediate-,
and high-NO_x conditions demonstrates that SICMA reproduces cumulative HCHO production and the evolution of OH and
330 HO₂ with good accuracy. Minor discrepancies arise in nighttime conditions due to the neglect of ozonolysis and the lumping
of intermediate oxidation products.

In global simulations for 2019, SICMA reproduces annual mean HCHO columns from the full chemistry within 10% over
most continental regions. Differences are largest over remote oceans, where reduced NO_x reservoir formation lowers back-
ground HCHO production, and over regions where emissions differ strongly from the assumed 10% monoterpene-to-isoprene

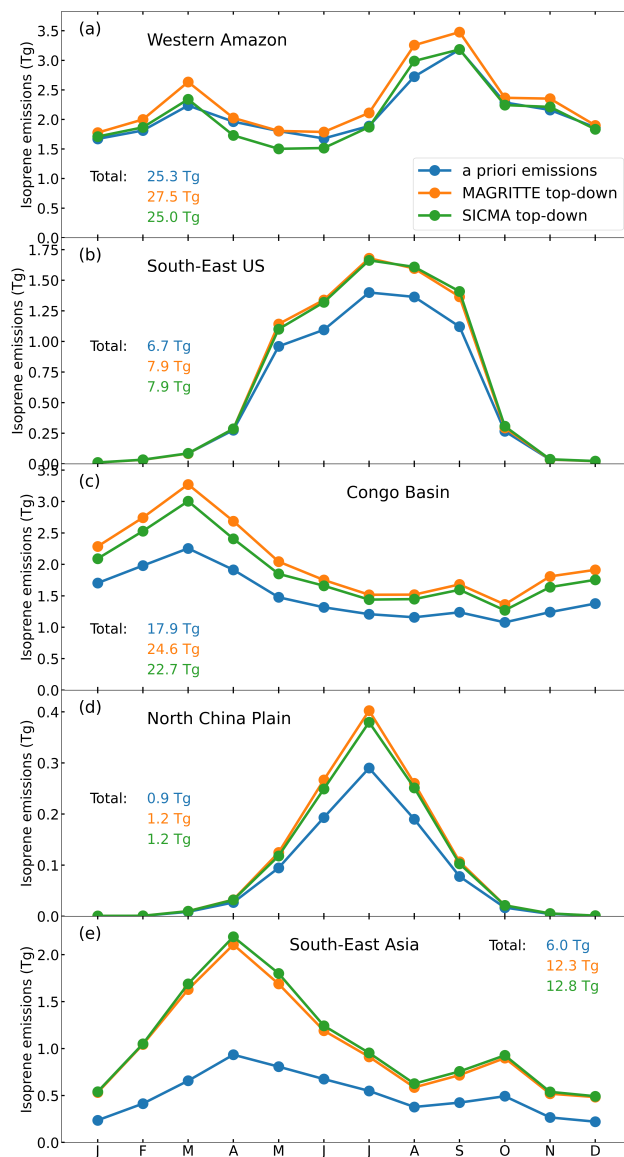


Figure 9. Monthly isoprene emissions for Western Amazon, South-East US, Congo Basin, North China Plain, and South-East Asia (from top to bottom) in 2019. The regions are defined in Fig. 1 and Fig. 6. The lines correspond to a priori emissions from MEGAN-MOHYCAN (blue), and top-down isoprene emissions from the MAGRITTE (orange) and SICMA (green) chemistry inversion runs.

335 molar ratio. Nevertheless, the seasonal cycle and regional patterns of HCHO columns are very similar between the two schemes and consistent with TROPOMI observations.

Adjoint-based inversions of isoprene emissions constrained by TROPOMI HCHO columns show low sensitivity to the chemical complexity of the mechanism. Both schemes increase global isoprene emissions from 439 Tg yr^{-1} (a priori) to



Table 4. Global annual emissions in Tg yr^{-1} of isoprene, biomass burning and anthropogenic VOC emissions in the bottom-up inventory (a priori) and according to the optimizations using either MAGRITTEv1.2 or SICMA chemistry for 2019.

Region	a priori	MAGRITTE (top-down)	SICMA (top-down)
Isoprene			
Global	439.2	568.4	568.0
Western Amazon	25.3	27.5	25.0
South-East US	6.7	7.9	7.9
Congo Basin	17.9	24.6	22.7
North China Plain	0.9	1.2	1.2
South-East Asia	6.0	12.3	12.8
Biomass burning VOCs			
Global	92.6	98.5	99.6
Western Amazon	1.0	1.0	1.0
South-East US	0.5	0.5	0.5
Congo Basin	2.7	2.6	2.6
North China Plain	1.2	1.2	1.2
South-East Asia	2.3	2.8	2.7
Anthropogenic VOCs			
Global	158.9	198.6	216.3
Western Amazon	0.1	0.1	0.1
South-East US	1.0	1.0	1.1
Congo Basin	0.9	0.9	0.9
North China Plain	9.8	16.3	18.4
South-East Asia	3.9	5.2	7.7

340 approximately 568 Tg yr^{-1} in 2019, with regional differences generally below 20%. SICMA thus retains the essential chemical behavior relevant for HCHO-based emission inversions while drastically reducing mechanism size. It provides an efficient alternative to detailed isoprene chemistry for ensemble simulations, sensitivity analyses, and data assimilation applications in global chemistry transport models.

As part of this work, the KPP-based optimization framework used to derive SICMA is made publicly available (Oomen, 2026). This framework enables the systematic derivation of reduced chemical mechanisms by optimizing stoichiometric coef-



345 ficients and reaction rates against a chosen reference scheme. For applications in other chemistry-transport models, users can recalibrate the simplified mechanism by constraining the optimization with box-model simulations from their own reference chemistry. This allows the construction of tailored simplified isoprene mechanisms that preserve key chemical features under different conditions and has been applied to IFS-COMPO chemistry (Williams et al., 2022) for the purpose of data assimilation of HCHO and isoprene emission inversion in the Copernicus Atmospheric Monitoring System (CAMS).

350 *Code and data availability.* The current version of the SICMA optimization software is available from <https://gitlab.aeronomie.be/ae/d23/kpp-based-optimization-of-simplified-chemistry-models>. The exact version of the model used to produce the results used in this paper is archived on Zenodo (<https://doi.org/10.5281/zenodo.19886691>, Oomen, 2026). The ESA CCI L3 TROPOMI HCHO dataset is available at De Smedt et al. (2025).

Author contributions. GMO designed the optimization software, carried out the analysis, and wrote the manuscript. JFM and TS designed the MAGRITTE chemistry-transport model and its inversion scheme. IDS produced the TROPOMI HCHO dataset and wrote Sect. 2. VH, 355 FK, AI, and JF provided valuable feedback and tested the simplified chemistry in CAMS. All authors read and commented on the manuscript.

Competing interests. The authors have no competing interests to declare.

Acknowledgements. This research was performed as part of the CAMEO project funded by the European Union (grant agreement No. 101082125, 2023–2025) and as part of the PIRAMID project funded by the European Space Agency (contract No. 4000147434/24/I-LR). 360 The ESA CCI L3 HCHO dataset was funded by the European Space Agency (contract No. 4000138243).



References

- Andreae, M. O.: Emission of trace gases and aerosols from biomass burning - an updated assessment, *Atmos. Chem. Phys.*, 19, 8523–8546, <https://doi.org/10.5194/acp-19-8523-2019>, 2019.
- Archibald, A. T., Jenkin, M. E., and Shallcross, D. E.: An isoprene mechanism intercomparison, *Atmos. Environ.*, 44, 5356–5364, <https://doi.org/10.1016/j.atmosenv.2009.09.016>, 2010.
- 365 Atkinson, R. and Arey, J.: Gas-phase tropospheric chemistry of biogenic volatile organic compounds: a review, *Atmos. Environ.*, 37, 197–219, [https://doi.org/10.1016/S1352-2310\(03\)00391-1](https://doi.org/10.1016/S1352-2310(03)00391-1), 2003.
- Bates, K. H. and Jacob, D. J.: A new model mechanism for atmospheric oxidation of isoprene: global effects on oxidants, nitrogen oxides, organic products, and secondary organic aerosol, *Atmos. Chem. Phys.*, 23, 9613–9640, <https://doi.org/doi:10.5194/acp-19-9613-2019>, 370 2019.
- Bauwens, M., Stavrakou, T., Müller, J.-F., De Smedt, I., Van Roozendael, M., van der Werf, G. R., Wiedinmyer, C., Kaiser, J. W., Sindelarova, K., and Guenther, A.: Nine years of global hydrocarbon emissions based on source inversion of OMI formaldehyde observations, *Atmos. Chem. Phys.*, 16, 10 133–10 158, <https://doi.org/10.5194/acp-16-10133-2016>, 2016.
- Burkholder, J. B., Sander, S. P., Abbatt, J. P. D., Barker, J. R., Huie, R. E., Kolb, C. E., Kurylo, M. J., Orkin, V. L., Wilmouth, D. M., and 375 Wine, P. H.: Chemical kinetics and photochemical data for use in atmospheric studies: evaluation number 18, <https://doi.org/2014/45510>, 2015.
- Claeys, M., Graham, B., Vas, G., Wang, W., Vermeylen, R., Pashynska, V., Cafmeyer, J., Guyon, P., Andreae, M. O., Artaxo, P., and Maenhaut, W.: Formation of Secondary Organic Aerosols Through Photooxidation of Isoprene, *Science*, 303, 1173–1176, <https://doi.org/10.1126/science.1092805>, 2004.
- 380 Compernelle, S., Lambert, J.-C., Verhoelst, T., Langerock, B., Pinardi, G., Sha, M. K., Krause, K., Richter, A., and Vigouroux, C.: Product Validation and Intercomparison Report, Tech. Rep. Precursors_cci+_D4.1_PVIR_02_00, ESA Climate Change Initiative (CCI+) Precursors Project, <https://climate.esa.int/en/projects/precursors-for-aerosols-and-ozone/>, issue 02, Revision 00, Status: Final, 2025.
- Darmenov, A. and da Silva, A.: The Quick Fire Emissions Dataset (QFED): Documentation of versions 2.1, 2.2 and 2.4, NASA Technical Report Series on Global Modeling and Data Assimilation NASA TM-2015-104606, 38, 2015.
- 385 De Smedt, I., Pinardi, G., Vigouroux, C., Compernelle, S., Bais, A., Benavent, N., Boersma, F., Chan, K.-L., Donner, S., Eichmann, K.-U., Hedelt, P., Hendrick, F., Irie, H., Kumar, V., Lambert, J.-C., Langerock, B., Lerot, C., Liu, C., Loyola, D., Piters, A., Richter, A., Rivera Cárdenas, C., Romahn, F., Ryan, R. G., Sinha, V., Theys, N., Vlietinck, J., Wagner, T., Wang, T., Yu, H., and Van Roozendael, M.: Comparative assessment of TROPOMI and OMI formaldehyde observations and validation against MAX-DOAS network column measurements, *Atmos. Chem. Phys.*, 21, 12 561–12 593, <https://doi.org/10.5194/acp-21-12561-2021>, 2021.
- 390 De Smedt, I., Vlietinck, J., YU, H., Theys, N., Danckaert, T., and Van Roozendael, M.: CCI+P HCHO tropospheric column L3 data from TROPOMI, v2, <https://doi.org/10.18758/Y591KDA5>, 2025.
- Gao, F. and Han, L.: Implementing the Nelder-Mead simplex algorithm with adaptive parameters, *Computational Optimization and Applications*, 51, 259–277, <https://doi.org/10.1007/s10589-010-9329-3>, 2012.
- Guenther, A. B., Jiang, X., Heald, C. L., Sakulyanontvittaya, T., Duhl, T., Emmons, L. K., and Wang, X.: The Model of Emissions of Gases and Aerosols from Nature version 2.1 (MEGAN2.1): an extended and updated framework for modeling biogenic emissions, *Geosci. Model Dev.*, 5, 1471–1492, <https://doi.org/10.5194/gmd-5-1471-2012>, 2012.



- Hersbach, H., Bell, B., Berrisford, P., Hirahara, S., Horányi, A., Muñoz-Sabater, J., Nicolas, J., Peubey, C., Radu, R., Schepers, D., Simmons, A., Soci, C., Abdalla, S., Abellan, X., Balsamo, G., Bechtold, P., Biavati, G., Bidlot, J., Bonavita, M., Chiara, G., Dahlgren, P., Dee, D., Diamantakis, M., Dragani, R., Flemming, J., Forbes, R., Fuentes, M., Geer, A., Haimberger, L., Healy, S., Hogan, R. J., Hólm, E., Janisková, M., Keeley, S., Laloyaux, P., Lopez, P., Lupu, C., Radnoti, G., Rosnay, P., Rozum, I., Vamborg, F., Villaume, S., and Thépaut, J.-N.: The ERA5 global reanalysis, *Q. J. Roy. Meteor. Soc.*, 146, 1999–2049, <https://doi.org/10.1002/qj.3803>, 2020.
- 400 Inness, A., Ades, M., Agustí-Panareda, A., Barré, J., Benedictow, A., Blechschmidt, A.-M., Dominguez, J. J., Engelen, R., Eskes, H., Flemming, J., Huijnen, V., Jones, L., Kipling, Z., Massart, S., Parrington, M., Peuch, V.-H., Razinger, M., Remy, S., Schulz, M., and Suttie, M.: The CAMS reanalysis of atmospheric composition, *Atmos. Chem. Phys.*, 19, 3515–3556, <https://doi.org/10.5194/acp-19-3515-2019>,
405 2019.
- Jenkin, M. E., Young, J. C., and Rickard, A. R.: The MCM v3.3.1 degradation scheme for isoprene, *Atmos. Chem. Phys.*, 15, 11 433–11 459, <https://doi.org/10.5194/acp-15-11433-2015>, <https://doi.org/10.5194/acpd-15-9709-2015>, 2015.
- Jenkin, M. E., Khan, M. A. H., Shallcross, D. E., Bergström, R., Simpson, D., Murphy, K. L. C., and Rickard, A. R.: The CRI v2.2 reduced degradation scheme for isoprene, *Atmos. Environ.*, 212, 172–182, <https://doi.org/10.1016/j.atmosenv.2019.05.055>, 2019.
- 410 Kaiser, J., Jacob, D. J., Zhu, L., Travis, K. R., Fisher, J. A., González Abad, G., Zhang, L., Zhang, X., Fried, A., Crouse, J. D., St. Clair, J. M., and Wisthaler, A.: High-resolution inversion of OMI formaldehyde columns to quantify isoprene emission on ecosystem-relevant scales: application to the southeast US, *Atmos. Chem. Phys.*, 18, 5483–5497, <https://doi.org/10.5194/acp-18-5483-2018>, 2018.
- Li, H., Ciais, P., Kumar, P., Hauglustaine, D. A., Chevallier, F., Broquet, G., Millet, D. B., Wells, K. C., Lian, J., and Zheng, B.: Global biogenic isoprene emissions 2013–2020 inferred from satellite isoprene observations, *Earth Syst. Sci. Data*, 17, 7035–7054, <https://doi.org/10.5194/essd-17-7035-2025>, 2025.
- 415 Li, H., Ciais, P., Kumar, P., Broquet, G., Chevallier, F., Hauglustaine, D. A., Millet, D. B., Wells, K. C., Lian, J., Bourtsoukidis, E., Zhang, K., and Zheng, B.: Contrasting Biogenic Isoprene Emission Responses to La Niña and El Niño Driven by Temperature: Insights from HCHO-Based Global Inversion, *Environ. Sci. Tech.*, 60, 3403–3415, <https://doi.org/10.1021/acs.est.5c12927>, PMID: 41554096, 2026.
- Millet, D. B., Jacob, D. J., Boersma, K. F., Fu, T.-M., Kurosu, T. P., Chance, K., Heald, C. L., and Guenther, A.: Spatial distribution of isoprene emissions from North America derived from formaldehyde column measurements by the OMI satellite sensor, *J. Geophys. Res.-Atmos.*, 113, D02307, <https://doi.org/10.1029/2007JD008950>, 2008.
- 420 Müller, J. F. and Stavrou, T.: Inversion of CO and NO_x emissions using the adjoint of the IMAGES model, *Atmos. Chem. Phys.*, 5, 1157–1186, <https://doi.org/10.5194/acp-5-1157-2005>, 2005.
- Müller, J.-F., Stavrou, T., Bauwens, M., Compernelle, S., and Peeters, J.: Chemistry and deposition in the Model of Atmospheric composition at Global and Regional scales using Inversion Techniques for Trace gas Emissions (MAGRITTE v1.0). Part B. Dry deposition, *Geoscientific Model Development Discussions*, 2018, 1–49, <https://doi.org/10.5194/gmd-2018-317>, 2018.
- 425 Müller, J. F., Stavrou, T., Bauwens, M., George, M., Hurtmans, D., Coheur, P. F., Clerbaux, C., and Sweeney, C.: Top-Down CO Emissions Based On IASI Observations and Hemispheric Constraints on OH Levels, *Geophysical Research Letters*, 45, 1621–1629, <https://doi.org/10.1002/2017GL076697>, 2018.
- 430 Müller, J.-F., Stavrou, T., and Peeters, J.: Chemistry and deposition in the Model of Atmospheric composition at Global and Regional scales using Inversion Techniques for Trace gas Emissions (MAGRITTE v1.1) - Part 1: Chemical mechanism, *Geosci. Model Dev.*, 12, 2307–2356, <https://doi.org/10.5194/gmd-12-2307-2019>, 2019.
- Müller, J.-F., Stavrou, T., Oomen, G.-M., Opacka, B., De Smedt, I., Guenther, A., Vigouroux, C., Langerock, B., Bauer Aquino, C. A., Grutter, M., Hannigan, J., Hase, F., Kivi, R., Lutsch, E., Mahieu, E., Makarova, M., Metzger, J.-M., Morino, I., Murata, I., Nagahama, T.,



- 435 Notholt, J., Ortega, I., Palm, M., Röhling, A., Stremme, W., Strong, K., Sussmann, R., Té, Y., and Fried, A.: Bias Correction Of Omi Hcho Columns Based On Ftir And Aircraft Measurements And Impact On Top-Down Emission Estimates, *Atmos. Chem. Phys.*, **24**, 2207–2237, <https://doi.org/10.5194/acp-24-2207-2024>, 2024.
- Novelli, A., Vereecken, L., Bohn, B., Dorn, H.-P., Gkatzelis, G. I., Hofzumahaus, A., Holland, F., Reimer, D., Rohrer, F., Rosanka, S., Taraborrelli, D., Tillmann, R., Wegener, R., Yu, Z., Kiendler-Scharr, A., Wahner, A., and Fuchs, H.: Importance of isomerization reac-
440 tions for OH radical regeneration from the photo-oxidation of isoprene investigated in the atmospheric simulation chamber SAPHIR, *Atmospheric Chemistry and Physics*, **20**, 3333–3355, <https://doi.org/10.5194/acp-20-3333-2020>, 2020.
- Oomen, G.-M.: SICMA v1.0.0 software, *Zenodo*, <https://doi.org/10.5281/zenodo.19886691>, 2026.
- Oomen, G.-M., Müller, J.-F., Stavrou, T., De Smedt, I., Blumenstock, T., Kivi, R., Makarova, M., Palm, M., Röhling, A., Té, Y., Vigouroux, C., Friedrich, M. M., Frieß, U., Hendrick, F., Merlaud, A., PETERS, A., Richter, A., Van Roozendaal, M., and Wagner, T.: Weekly derived
445 top-down volatile-organic-compound fluxes over Europe from TROPOMI HCHO data from 2018 to 2021, *Atmos. Chem. Phys.*, **24**, 449–474, <https://doi.org/10.5194/acp-24-449-2024>, 2024.
- Opacka, B., Stavrou, T., Müller, J.-F., De Smedt, I., van Geffen, J., Marais, E. A., Horner, R. P., Millet, D. B., Wells, K. C., and Guenther, A. B.: Natural emissions of VOC and NO_x over Africa constrained by TROPOMI HCHO and NO₂ data using the MAGRITTEv1.1 model, *Atmos. Chem. Phys.*, **25**, 2863–2894, <https://doi.org/10.5194/acp-25-2863-2025>, 2025.
- 450 Palmer, P. I., Abbot, D. S., Fu, T.-M., Jacob, D. J., Chance, K., Kurosu, T. P., Guenther, A., Wiedinmyer, C., Stanton, J. C., Pilling, M. J., Pressley, S. N., Lamb, B., and Sumner, A. L.: Quantifying the seasonal and interannual variability of North American isoprene emissions using satellite observations of the formaldehyde column, *J. Geophys. Res.-Atmos.*, **111**, D12315, <https://doi.org/10.1029/2005JD006689>, 2006.
- Paulson, S. E. and Orlando, J. J.: The reactions of ozone with alkenes: An important source of HO_x in the boundary layer, *Geophys. Res. Lett.*, **23**, 3727–3730, <https://doi.org/10.1029/96GL03477>, 1996.
455
- Peeters, J., Nguyen, T. L., and Vereecken, L.: HO_x radical regeneration in the oxidation of isoprene, *Phys. Chem. Chem. Phys.*, **11**, 5935, <https://doi.org/10.1039/b908511d>, 2009.
- Peeters, J., Müller, J.-F., Stavrou, T., and Nguyen, V. S.: Hydroxyl Radical Recycling in Isoprene Oxidation Driven by Hydrogen Bonding and Hydrogen Tunneling: The Upgraded LIM1 Mechanism, *J. Phys. Chem. A*, **118**, 8625–8643, <https://doi.org/10.1021/jp5033146>, 2014.
- 460 Sandu, A., Sander, R., Long, M. S., Yantosca, R. M., Lin, H., Shen, L., and Jacob, D. J.: KineticPreProcessor/KPP: The Kinetic PreProcessor (KPP) 3.0.2, <https://doi.org/10.5281/zenodo.8030063>, 2023.
- Sfendla, Y., Stavrou, T., Müller, J.-F., Oomen, G.-M., Opacka, B., Danckaert, T., De Smedt, I., and Lerot, C.: Global VOC emissions quantified from inversion of TROPOMI spaceborne formaldehyde and glyoxal data, *Atmos. Chem. Phys.*, **26**, 733–767, <https://doi.org/10.5194/acp-26-733-2026>, 2026.
- 465 Sindelarova, K., Markova, J., Simpson, D., Huszar, P., Karlicky, J., Darras, S., and Granier, C.: High-resolution biogenic global emission inventory for the time period 2000–2019 for air quality modelling, *Earth Syst. Sci. Data*, **14**, 251–270, <https://doi.org/10.5194/essd-14-251-2022>, 2022.
- Soulie, A., Granier, C., Darras, S., Zilbermann, N., Doumbia, T., Guevara, M., Jalkanen, J.-P., Keita, S., Lioussé, C., Crippa, M., Guizzardi, D., Hoesly, R., and Smith, S. J.: Global Anthropogenic Emissions (Cams-Glob-Ant) For The Copernicus Atmosphere Monitoring Service
470 Simulations Of Air Quality Forecasts And Reanalyses, *Earth System Science Data*, **16**, 2261–2279, <https://doi.org/10.5194/essd-16-2261-2024>, 2024.



- Stavrakou, T., Müller, J. F., de Smedt, I., van Roozendaal, M., Kanakidou, M., Vrekoussis, M., Wittrock, F., Richter, A., and Burrows, J. P.: The continental source of glyoxal estimated by the synergistic use of spaceborne measurements and inverse modelling, *Atmos. Chem. Phys.*, 9, 8431–8446, <https://doi.org/10.5194/acp-9-8431-2009>[10.5194/acpd-9-13593-2009](https://doi.org/10.5194/acpd-9-13593-2009), 2009a.
- 475 Stavrakou, T., Müller, J. F., de Smedt, I., van Roozendaal, M., van der Werf, G. R., Giglio, L., and Guenther, A.: Global emissions of non-methane hydrocarbons deduced from SCIAMACHY formaldehyde columns through 2003–2006, *Atmos. Chem. Phys.*, 9, 3663–3679, <https://doi.org/10.5194/acp-9-3663-2009>[10.5194/acpd-9-4609-2009](https://doi.org/10.5194/acpd-9-4609-2009), 2009b.
- Stavrakou, T., Müller, J. F., Bauwens, M., De Smedt, I., Van Roozendaal, M., De Mazière, M., Vigouroux, C., Hendrick, F., George, M., Clerbaux, C., Coheur, P. F., and Guenther, A.: How consistent are top-down hydrocarbon emissions based on formaldehyde observations
480 from GOME-2 and OMI?, *Atmos. Chem. Phys.*, 15, 11 861–11 884, <https://doi.org/10.5194/acp-15-11861-2015>, 2015.
- Stavrakou, T., Müller, J. F., Bauwens, M., De Smedt, I., Van Roozendaal, M., and Guenther, A.: Impact of Short-Term Climate Variability on Volatile Organic Compounds Emissions Assessed Using OMI Satellite Formaldehyde Observations, *Geophys. Res. Lett.*, 45, 8681–8689, <https://doi.org/10.1029/2018GL078676>, 2018.
- Sun, S., Palmer, P. I., Siddans, R., Kerridge, B. J., Ventress, L., Edtbauer, A., Ringsdorf, A., Pfannerstill, E. Y., and Williams, J.: Seasonal
485 isoprene emission estimates over tropical South America inferred from satellite observations of isoprene, *Atmos. Chem. Phys.*, 25, 15 801–15 818, <https://doi.org/10.5194/acp-25-15801-2025>, 2025.
- Tilstra, L. G., de Graaf, M., Trees, V. J. H., Litvinov, P., Dubovik, O., and Stammes, P.: A Directional Surface Reflectance Climatology Determined From Tropomi Observations, *Atmos. Meas. Tech.*, 17, 2235–2256, <https://doi.org/10.5194/amt-17-2235-2024>, 2024.
- Van Roozendaal, M., Boersma, F., Seo, S., Valks, P., De Smedt, I., Theys, N., Hedelt, P., Danckaert, T., Clarisse, L., Van Damme, M.,
490 Clerbaux, C., and George, M.: Algorithm Theoretical Basis Document, Tech. Rep. Precursors_cci+_D2.1_ATBD_02_04, ESA Climate Change Initiative (CCI+) Precursors Project, <https://climate.esa.int/en/projects/precursors-for-aerosols-and-ozone/>, issue 02, Revision 04, Status: Final (corrected for RIDs), 2026.
- Vigouroux, C., Langerock, B., Bauer Aquino, C. A., Blumenstock, T., Cheng, Z., De Mazière, M., De Smedt, I., Grutter, M., Hannigan, J. W., Jones, N., Kivi, R., Loyola, D., Lutsch, E., Mahieu, E., Makarova, M., Metzger, J.-M., Morino, I., Murata, I., Nagahama, T., Notholt, J.,
495 Ortega, I., Palm, M., Pinardi, G., Röhlings, A., Smale, D., Stremme, W., Strong, K., Sussmann, R., Té, Y., van Roozendaal, M., Wang, P., and Winkler, H.: TROPOMI-Sentinel-5 Precursor formaldehyde validation using an extensive network of ground-based Fourier-transform infrared stations, *Atmos. Meas. Tech.*, 13, 3751–3767, <https://doi.org/10.5194/amt-13-3751-2020>, 2020.
- Wells, K. C., Millet, D. B., Payne, V. H., Deventer, M. J., Bates, K. H., de Gouw, J. A., Graus, M., Warneke, C., Wisthaler, A., and Fuentes, J. D.: Satellite isoprene retrievals constrain emissions and atmospheric oxidation, *Nature*, 585, 225–233, <https://doi.org/10.1038/s41586-020-2664-3>, 2020.
500
- Wennberg, P. O., Bates, K. H., Crouse, J. D., Dodson, L. G., McVay, R. C., Mertens, L. A., Nguyen, T. B., Praske, E., Schwantes, R. H., Smarte, M. D., St Clair, J. M., Teng, A. P., Zhang, X., and Seinfeld, J. H.: Gas-Phase Reactions of Isoprene and Its Major Oxidation Products, *Chem. Rev.*, 118, 3337–3390, <https://doi.org/10.1021/acs.chemrev.7b00439>, PMID: 29522327, 2018.
- Williams, J. E., Huijnen, V., Bouarar, I., Meziane, M., Schreurs, T., Pelletier, S., Marécal, V., Josse, B., and Flemming, J.: Regional evaluation
505 of the performance of the global CAMS chemical modeling system over the United States (IFS cycle 47r1), *Geosci. Model Dev.*, 15, 4657–4687, <https://doi.org/10.5194/gmd-15-4657-2022>, 2022.
- Wiser, F., Place, B. K., Sen, S., Pye, H. O. T., Yang, B., Westervelt, D. M., Henze, D. K., Fiore, A. M., and McNeill, V. F.: AMORE-Isoprene v1.0: a new reduced mechanism for gas-phase isoprene oxidation, *Geosci. Model Dev.*, 16, 1801–1821, <https://doi.org/10.5194/gmd-16-1801-2023>, 2023.